ELSEVIER

Polymer 41 (2000) 7139–7145

polymer

The effects of stress relaxation on the structure and orientation of tensile drawn poly(ethylene terephthalate)

R.G. Matthews[a], A. Ajji[a,*], M.M. Dumoulin[a], R.E. Prud'homme[b]

[a]*Industrial Materials Institute, National Research Council Canada, 75 Boul. de Mortagne, Boucherville, Que., Canada J4B 6Y4*
[b]*CERSIM et Département de Chimie, Université Laval, Que., Canada G1K 7P4*

Received 21 July 1999; received in revised form 28 December 1999; accepted 30 December 1999

Abstract

Tensile drawing experiments on poly(ethylene terephthalate) (PET) have shown that there is no significant strain-induced crystallisation until draw ratios around 2.3. The actual onset of strain-induced crystallisation depends on the deformation rate, and it occurs at lower draw ratios for higher draw rates. The development of strain-induced crystallisation has a significant impact on the relaxation behaviour of PET. Online birefringence measurements, during the relaxation of PET drawn to different draw ratios showed that: (a) at low draw ratios, the orientation relaxes over long periods of time and Fourier transform infrared (FTIR) spectroscopy showed that the overall orientation falls after relaxation; (b) at higher draw ratios, when significant strain-induced crystallisation has occurred, the orientation decreases over short times, of the order of 10 s and remains constant thereafter. This behaviour is probably due to the crystallites that lock in the extension of the chains in the amorphous material. Post relaxation FTIR measurements showed that the orientation increases due to annealing effect. Differential scanning calorimetry (DSC) showed that there is an increase in the crystalline fraction after relaxation for all draw ratios, which is probably due to the conversion of oriented amorphous material (*trans* conformers) into the crystalline phase.

Keywords: Poly(ethylene terephthalate); Orientation; Relaxation

1. Introduction

Poly(ethylene terephthalate) (PET) is a semi-crystalline polymer of considerable commercial importance that, when oriented, has a variety of applications in film, fibre or bottle form. Orientation can be produced using many techniques, including tensile drawing, roll drawing, blow moulding and solid state extrusion [1–5]. The level of orientation obtained from these techniques is reduced by relaxation, the recovery that occurs when the deforming force is removed. Recovery has been attributed to motions of the polymer chains in the amorphous regions [6], which reduces the extension of the chains. The oriented chains tend to the isotropic state because this is the most energetically favourable state. Efforts to maximise the orientation produced during processing would benefit from a more detailed understanding of the relaxation mechanisms.

Roll drawing has been of great interest to this group. The relationship between the major processing parameters and the resulting oriented material structure and properties were studied [7,8]. It was shown that orientation could be increased by increasing the roll speed, or by reducing the roll gap. A feature of the process, which was observed but not examined in detail, was the significant loss of orientation due to relaxation. It is a major factor because the deforming force is totally removed as the film leaves the roll, which allows essentially free relaxation. The recovery process was not examined directly, during roll drawing, because stress and orientation measurements are difficult to obtain in this situation. While orientation measurements are theoretically possible, such measurements close to the rolls, where the majority of the recovery occurs, are technically difficult to achieve. For this reason, it was decided that the deformation and relaxation processes should be examined in a simpler situation. The effectiveness of applying tension to the oriented film, after the final roll, in reducing recovery is investigated in a separate paper [9].

Under tensile drawing conditions, it is relatively simple to make stress and orientation measurements, during both the drawing and relaxation. In this study, the relaxation behaviour was studied for samples held at constant length, while maintained at the drawing temperature. To examine the

* Corresponding author. Tel.: + 1-450-641-5244; fax: + 1-450-641-5105.
E-mail address: abdellah.ajji@nrc.ca (A. Ajji).

0032-3861/00/$ - see front matter
PII: S0032-3861(00)00052-5

effects of relaxation on the final oriented material, two sets of samples were produced. After drawing, some samples were quenched rapidly to minimise relaxation; these samples are called 'as-drawn'. The second set of samples, on which the online measurements were made, were allowed to relax for 30 min; these samples are called 'relaxed'. The orientation was measured by birefringence and Fourier transform infrared spectroscopy. A comparison between the structure and the orientation of the as-drawn and relaxed samples was made, and differences discussed.

2. Experimental details

The polymer studied was Du Pont Selar PT 7086 PET, an extrusion grade without nucleating agent. The manufacturer quotes an intrinsic viscosity (IV) of 1.0. The molecular weight characteristics, obtained using gel permeation chromatography (GPC) relative to polystyrene standards, are $M_n = 28,000$ and $M_w = 54,600$. Amorphous sheets were produced by compressing dried PET granules in a hot press, at 280°C, then quenching the melt by immersion in water. The samples were oriented by drawing, at 80°C, on an Instron tensile testing machine.

As-drawn samples: cooled below the glass transition temperature (T_g) as soon as the extension was completed. *Relaxed samples:* the drawing temperature was maintained for 30 min, while leaving the samples at constant length, before cooling below T_g.

A spectrographic technique was used to measure the birefringence both on-line and off-line. The sample is placed between parallel polarisers, so that the light from a multi-wavelength source passes through the polarisers and the sample. A diffraction grating is used to disperse the spectrum of the transmitted light across a photodiode array. The intensity versus wavelength data, stored on a computer connected to the photodiode array, is used to calculate the retardation (retardation (Γ) = sample thickness (d) × birefringence (Δn)). All the measurements presented here were performed real-time upon draw or relaxation at constant length at 80°C. A more detailed description of the technique can be found elsewhere [10,11].

The crystalline fraction of the samples was measured using a Perkin–Elmer DSC 7 differential scanning calorimeter, scanning at 20°C/min. In calculating the crystalline fraction, the enthalpy of melting (ΔH_m), for fully crystallised PET, was assumed to be 140 J/g [12]. To take into account crystallisation during the scan, the area of the crystallisation exotherm was subtracted from the area of the melting endotherm.

Infrared dichroism measurements were made using front surface reflectance Fourier transform infrared (FTIR) spectroscopy. The spectra were obtained from a Nicolet 170SX spectrometer, with a resolution of 4 cm^{-1}, at a low angle of incidence in the specular (external) reflection mode. Spectra were measured in two orthogonal directions, parallel and perpendicular to the draw direction, without changing the sample position. To improve the spectra quality, the back surface of the samples was scratched to reduce the back surface reflections. The Kramers–Kronig transformation was performed, with the Spectra Calc Software™, using a MacLaurins series algorithm to perform the integration. The spectra were normalised by examining the 1410 cm^{-1} peak, which is insensitive to orientation and crystallinity [13].

The scope of this paper does not require a detailed discussion of the molecular motions responsible for the PET IR bands; a considerable body of literature deals directly with this subject [14–19]. Structural factor spectra, which are the spectra that would be observed if the oriented samples were actually isotropic, were obtained from the FTIR scans using the following equation:

$$\phi_0 = \left(\frac{\phi_\parallel + 2\phi_\perp}{3} \right) \tag{1}$$

where the symbols $\phi_\parallel$ and $\phi_\perp$ refer to the polarisability functions, which is more representative than the absorbencies [20], with the polarisation directions parallel and perpendicular to the draw direction, respectively. Orientation functions $\langle P_2(\cos\theta)\rangle$ were calculated, from the polarisability function spectra, using the following equation [20]:

$$\langle P_2(\cos\theta)\rangle = \frac{D-1}{D+2} \times \frac{2}{3\cos^2\alpha - 1} \tag{2}$$

where D is the dichroic ratio. The dichroic ratio for a given band is defined as the ratio of the peak areas obtained with the polarisation parallel and perpendicular to the draw direction ($A_\parallel/A_\perp$). For the bands examined in these experiments α equals: 21° for the 1340 cm^{-1} band, 20° for the 1020 cm^{-1} band and 90° for the 730 cm^{-1} band. The orientations' functions defined here are with respect to the drawing axis.

Orientation functions were also calculated using a second technique, which uses band heights in the reflectance spectra. The 1330–1240 and 1730 cm^{-1} reflectance bands show parallel and perpendicular dichroism, respectively. Cole et al. [20] have shown that this dichroism can be related to the overall orientation:

$$f_{c,J} = \frac{R_J - 1.12}{0.657 + 0.528R_J} \tag{3}$$

where R_J is the ratio of the heights of the reflectance peaks at 1243 and 1717 cm^{-1}, for a spectrum measured in the J-direction and $f_{c,J}$ is the orientation function of the chain axis with respect to the J-direction. Using Eq. (3), Cole et al. [20] were able to calculate overall orientation functions, with respect to the measurement directions, in uniaxially or biaxially oriented samples.

3. Results and discussion

In order to consider the effect of crystallinity on the PET

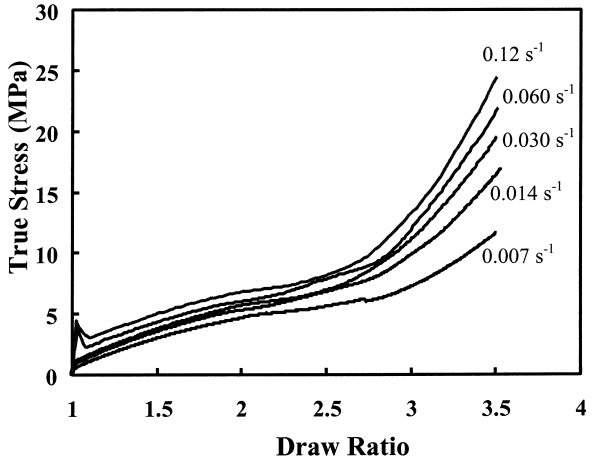

Fig. 1. True stress (MPa)–strain curves from drawing amorphous PET at 80°C at different initial strain rates as indicated (values are in s^{-1}) to $\lambda = 3.6$.

relaxation behaviour, birefringence was monitored at two different draw ratios, $\lambda = 2.0$ and 3.6. At $\lambda = 2.0$, there is significant orientation, but almost no strain-induced crystallisation; these samples are essentially amorphous. At $\lambda = 3.6$ (the highest draw ratio obtainable on the birefringence rig), there is significant orientation and crystallisation.

True stress–strain curves, from the drawing of PET at 80°C, are shown in Fig. 1. In these tests, amorphous PET samples were drawn to $\lambda = 3.6$ at different initial strain rates. At low rates, there is no peak in the true stress, and a rubber-like behaviour is observed. At high rates, there is a peak in the true stress, which corresponds to the onset of necking. The magnitude of the stress peak also increases with the rate. Over the remainder of the true stress–strain curves, the true stress increases with strain rate, particularly above a draw ratio of 2.5 (when crystallinity starts to develop). This is in agreement with previous work on PET [21–23].

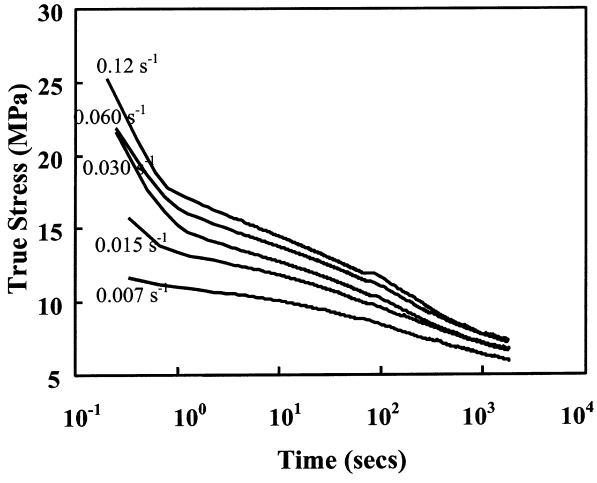

Fig. 2. Stress relaxation curves of samples drawn at 80°C at different initial strain rates as indicated (values are in s^{-1}) to $\lambda = 3.6$.

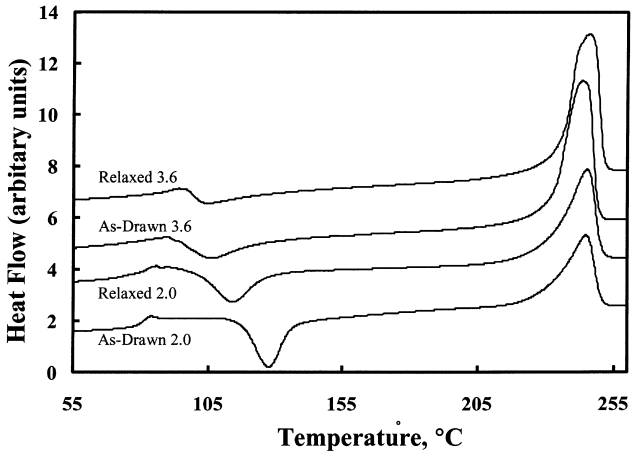

Fig. 3. DSC scans for as-drawn and relaxed PET samples drawn at 80°C and 0.007 s^{-1} to $\lambda = 2.0$ and 3.6.

Stress relaxation curves, obtained after drawing to $\lambda = 3.5$ at 80°C, are shown in Fig. 2. The true stress is plotted against the logarithm of the relaxation time. All the samples, independent of draw rate, show three regions to these curves. The true stress decreases continually, but the rate of decrease is greatest at times below 1 s. This is probably due to the rapid recovery of a viscous contribution to the drawing stress, which has been observed by several workers [24–26]. The magnitude of the initial fall in stress also increases with draw rate, which is indicative of viscous behaviour. At times between 1 and 10 s, the true stress decreases at a significantly lower rate and, at longer times, the rate again increases. The curves are not linear, which means that the relaxation is not caused by a single rate activated process. At $\lambda = 2.0$, the stress relaxation curves were essentially the same as at $\lambda = 3.6$, so they are not shown here.

Fig. 3 shows the DSC scans from as-drawn and relaxed PET samples drawn at 80°C and 0.007 s^{-1} to $\lambda = 2.0$ and 3.6. The melting endotherms, at 250°C, is larger at the higher draw ratio, indicating a higher crystalline fraction. At both draw ratios, the relaxation produces an increase in the crystallinity as explained below. The DSC scans show an exotherm at 90–120°C that corresponds to the crystallisation of oriented amorphous material. This is less significant at the higher draw ratio because more of the oriented material is crystallised during drawing. At the higher draw ratio, the crystallisation occurs at a lower temperature because the energy, required for crystallisation, decreases as the chains become more oriented. These features have all been reported in previous works [27–30]. Relaxation lowers the crystallisation temperature and decreases the magnitude of crystallisation exotherm. This suggests that oriented amorphous material was converted into crystalline material during the relaxation.

In Fig. 4, the crystalline fraction, as determined by DSC, is plotted against draw ratio, for PET drawn at 80°C and an initial strain rate of 0.007 s^{-1}. This shows that crystallinity

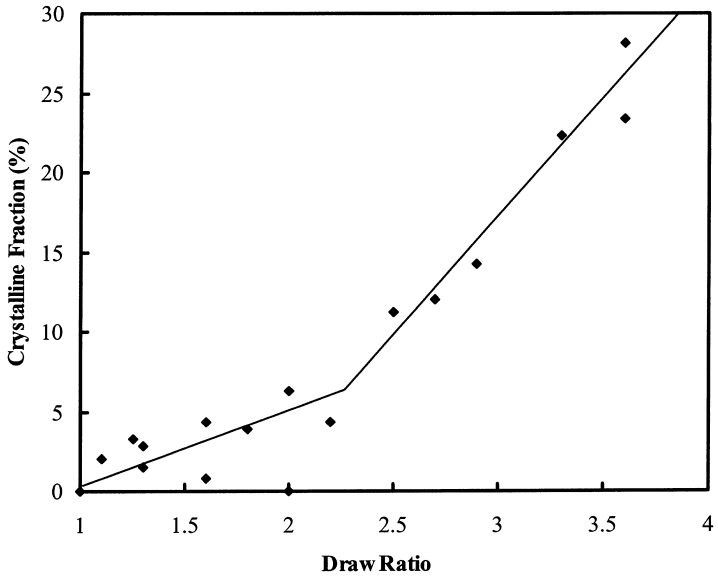

Fig. 4. Draw ratio dependence of crystalline fraction for as-drawn PET drawn at 80°C and 0.007 s^{-1}.

increases at a higher rate for draw ratios above 2.3. This is in line with previous works [21–24,26–30], showing that significant strain-induced crystallisation occurs only at draw ratios above 2.3. This also agrees with the stress behaviour, described above.

Fig. 5 shows the online birefringence measurements made during the drawing of amorphous PET at 80°C to $\lambda = 3.6$. For all strain rates, the birefringence increases with draw ratio. For draw ratios above 2.0, there is a greater increase in the gradient, which is probably due to the onset of strain-induced crystallisation. This gradient increase moves to lower draw ratios as the strain rate increases which suggests that strain-induced crystallisation occurs at lower draw ratios.

The online birefringence measurements made during stress relaxation, at $\lambda = 3.6$, are shown in Fig. 6. The birefringence initially decreases, for times up to 30 s but, at longer times, it becomes constant, although the stress continues to decrease. It is believed that some of the oriented amorphous chains can crystallise during the initial relaxation period but, at longer times, the birefringence remains constant because the crystallisation, significant at $\lambda = 3.6$, inhibits further relaxation. The crystallites anchor the amorphous chains in place, reducing the freedom of the chains to move, and so reducing the effects of the relaxation. Online birefringence data, from the relaxation at $\lambda = 2.0$, is shown in Fig. 7. For all the drawing rates, the birefringence decreases almost linearly with the logarithm of time. No plateau is seen at longer times due to the low level of strain-induced crystallisation at $\lambda = 2.0$ as discussed above.

Fig. 8 shows the dependence of the orientation functions of three specific vibrations calculated from the polarisability

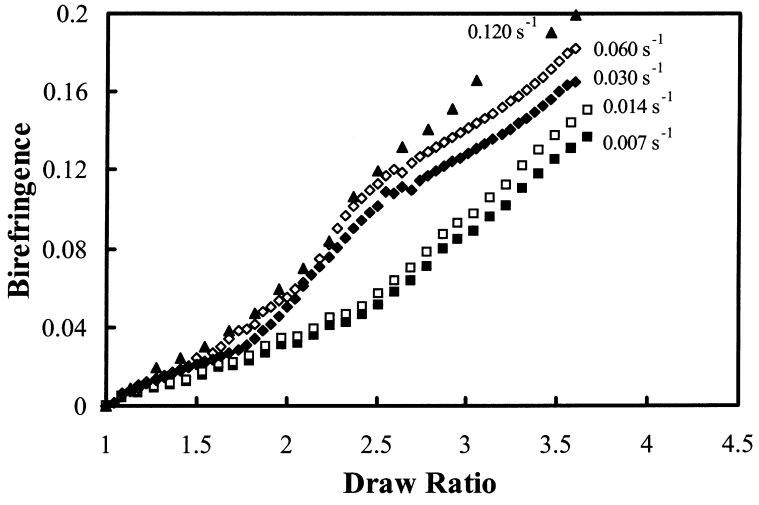

Fig. 5. Birefringence measured online during the drawing of amorphous PET at 80°C and at different strain rates as indicated.

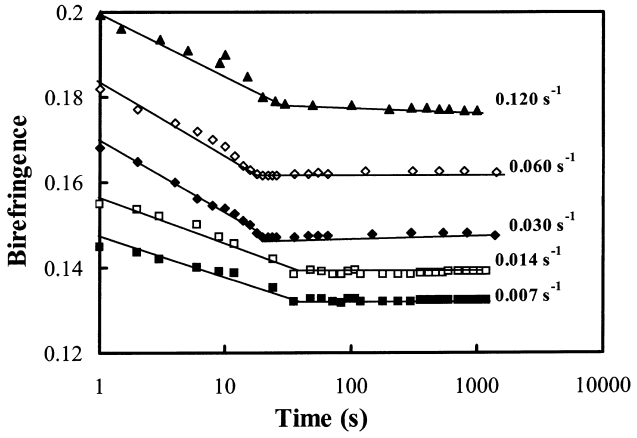

Fig. 6. Birefringence measured online during stress relaxation of PET drawn at 80°C and different strain rates to $\lambda = 3.6$.

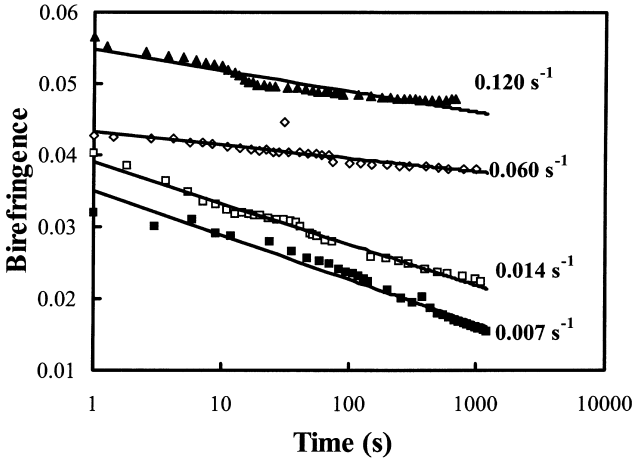

Fig. 7. Birefringence measured online during stress relaxation of PET drawn at 80°C and different strain rates to $\lambda = 2.0$.

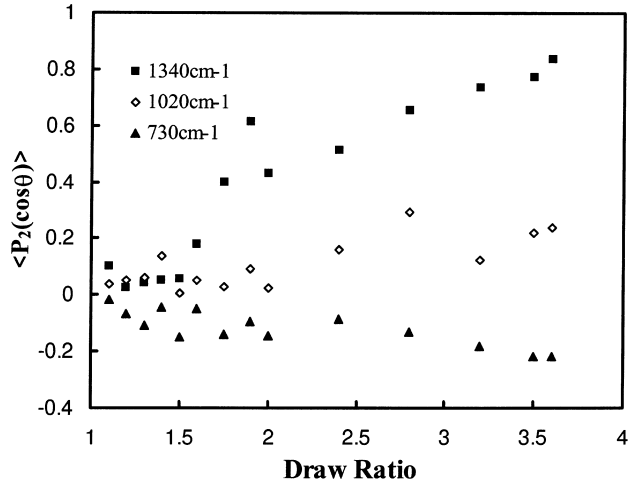

Fig. 8. Draw ratio dependence of orientation functions using three different bands as indicated, calculated from polarisability function spectra for as-drawn PET drawn at 80°C and 0.007 s^{-1}.

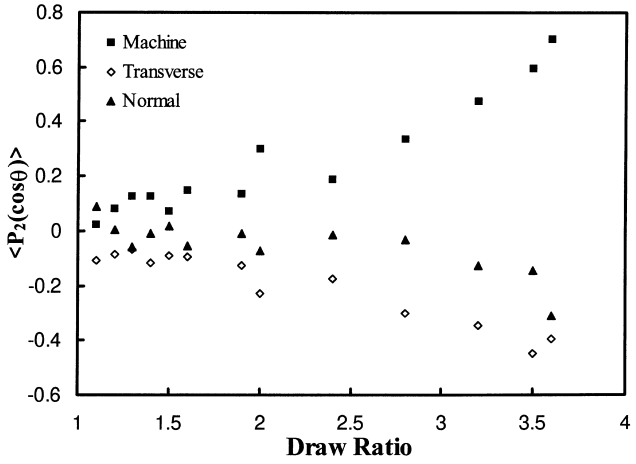

Fig. 9. Draw ratio dependence of the orientation functions using the 1340 cm^{-1} calculated from the reflection spectra, Eq. (2), for as-drawn PET drawn at 80°C and 0.007 s^{-1}.

function spectra on the draw ratio. The orientation functions of the 1340 and 1020 cm^{-1} bands increases with the draw ratio, but that for the 730 cm^{-1} band decreases. It has been shown [14] that the 1340 cm^{-1} band corresponds to wagging of the CH_2 units in the *trans* conformation; the increase in this orientation function indicates greater orientation of *trans* units in the draw direction. The 1020 and 730 cm^{-1} bands have both been assigned to motions of the hydrogen atoms on the benzene ring [14], in-plane and out-of-plane motions, respectively. During drawing, the polymer chains and, therefore, the planes of the benzene rings were oriented towards the draw direction. The 1020 cm^{-1} orientation function increases because the in-plane motions, responsible for the band, are also aligned with the draw direction; the 730 cm^{-1} orientation function decreases because the out-of-plane direction is increasingly oriented perpendicular to the

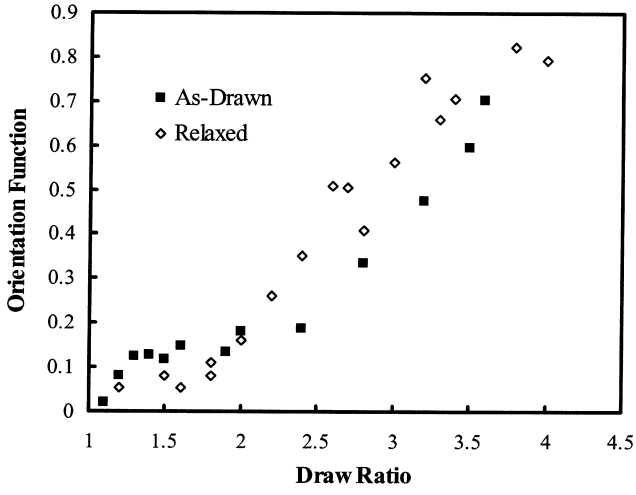

Fig. 10. Draw ratio dependence of the orientation functions in the machine direction using the 1340 cm^{-1} calculated from the reflectance spectra, Eq. (2), for as-drawn and relaxed PET drawn at 80°C and 0.007 s^{-1}.

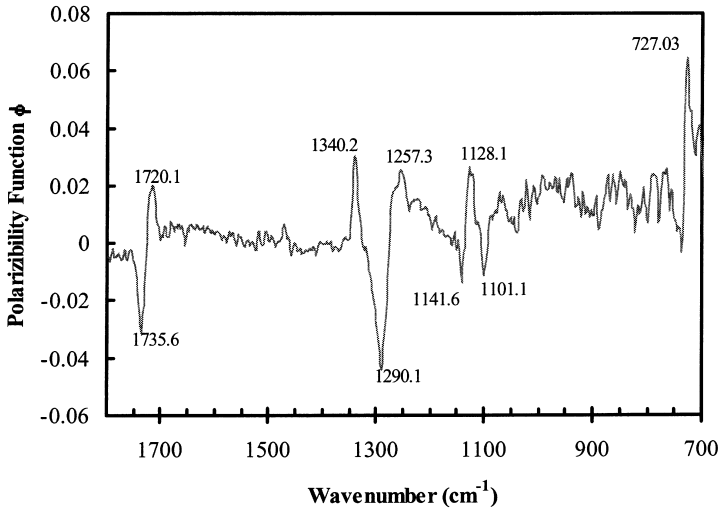

Fig. 11. Difference between the structural factor spectra (3.6–2.0) for as-drawn PET drawn at 80°C and 0.007 s^{-1} to $\lambda = 2.0$ and 3.6.

draw direction. Up to a draw ratio of 1.5, the changes in the orientation functions are small but, then, the orientation increases more rapidly.

Orientation functions were also calculated using the ratio of the 1330–1240 and 1729 cm^{-1} bands [20], because the orientation functions for the three axial directions can be obtained easily. The draw ratio dependencies of these orientation functions, representative of the chain axis orientation, obtained from the samples of as-drawn PET, are shown in Fig. 9. The orientation increases in the draw direction but decreases in the transverse and normal directions. These samples were drawn uniaxially, so the orientation functions for the transverse and normal directions are expected to decrease by the same amount; which is observed given the scatter in the experimental data. The changes in orientation are small up to $\lambda = 2.0$ but, then, the change is more rapid. This behaviour is similar to that observed in online birefringence measurements.

In Fig. 10, the draw ratio dependence of orientation is shown for as-drawn and relaxed samples, where the orientation functions correspond to orientation in the draw direction (from the 1340 cm^{-1}). At low draw ratios, the orientation function is higher for the as-drawn samples, because no or little relaxation occurred yet as compared to the relaxed samples, whereas the driving force towards the isotropic state is larger during relaxation. At high draw ratios, however, the strain-induced crystallites hinder the relaxation that can occur during the 30 min period when the samples are left at 80°C and, in addition, even if there is some loss of orientation in the amorphous regions, the increased orientation in the crystalline regions led to an increase in the orientation function.

Finally, Fig. 11 shows the difference spectrum between the structural factor spectra of as-drawn samples with draw ratios of 3.6 and 2.0 (the polarisability function at $\lambda = 2.0$ is subtracted from that at $\lambda = 3.6$). The minimum in the difference spectrum seen for the 1290 cm^{1} band, which is mainly due to motions in the amorphous regions, shows that there is a lower amorphous content at the higher draw ratio. The peak at 1720 cm^{-1} and the minimum at 1735 cm^{-1} also show that there is a higher amorphous content for the draw ratio of 2.0. The difference between the structural spectra for relaxed samples with draw ratios of 3.6 and 2.0 shows similar behaviour.

4. Conclusions

This work has shown that the relaxation of PET depends strongly on the final draw ratio reached. At high draw ratios, the birefringence does not decrease smoothly as occurs at low draw ratios, but becomes constant after a short time. This behaviour is due to the presence of strain-induced crystallisation. Significant strain-induced crystallisation occurs at draw ratios of about 2–2.3, but this also depends on the deformation rate. As the deformation rate is increased, crystallisation is seen at lower draw ratios. The crystallisation changes the relaxation behaviour because the crystallites lock the oriented chains in the drawn direction, which inhibits the conformational changes that are responsible for the relaxation.

Acknowledgements

The authors wish to acknowledge the financial support provided by the Natural Sciences and Engineering Research Council of Canada through a Strategic Grant for this work.

References

[1] Zachariades AE, Porter RS. The strength and stiffness of polymers. New York: Marcel Dekker, 1983.
[2] Zachariades AE, Porter RS. High modulus polymers. New York: Marcel Dekker, 1988.

[3] Ward IM. Structure and properties of oriented polymers. 2nd ed.. London: Chapman and Hall, 1997.
[4] New advances in oriented polymers, Proceedings of SPE RETEC, Atlantic City, NJ, September 1987.
[5] Ward IM. Adv Polym Sci 1985;70:1.
[6] Gupta VB, Radhakrishnan J, Sett SK. Polymer 1993;34:3814.
[7] Ajji A, Dufour J, Legros N, Dumoulin MM. J Reinf Plas Comp 1996;15:652.
[8] Ajji A, Legros N, Dumoulin MM. Proceedings of the Composites'96/ Oriented Polymers Symposium 9–11 October, Boucherville, Canada, 1996.
[9] Matthews RG, Ajji A, Dumoulin MM, Prud'homme RE. Polym Engng Sci 1999;39:2377.
[10] Ajji A, Guèvremont J, Matthews RG, Dumoulin MM. SPE ANTEC Proceedings, Atlanta, GA, USA, vol. 2, 1998. p. 1588.
[11] Beekmans F, Posthuma de Boer A. Macromolecules 1996;29:8726.
[12] Wunderlich B. Polym Engng Sci 1978;18:431.
[13] Walls DJ. Appl Spectrosc 1991;7:1193.
[14] Daniels WW, Kitson RE. J Polym Sci 1958;33:161.
[15] Bahl SK, Cornell DD, Boerio FJ, McGraw GE. J Polym Sci Polym Lett Ed 1974;12:13.
[16] Boerio FJ, Bahl SK, McGraw GE. J Polym Sci Polym Phys Ed 1976;14:1029.
[17] Ward IM, Wilding MA. Polymer 1977;18:327.
[18] Cole KC, Guèvremont J, Ajji A, Dumoulin MM. Appl Spectrosc 1994;48(12):1513.
[19] Krimm S. Adv Polym Sci 1960;2:51.
[20] Cole KC, Ben Daly H, Sanschagrin B, Nguyen KT. Polymer 1999;40:3505.
[21] Matthews RG, Duckett RA, Ward IM, Jones DP. Polymer 1997;38(19):4795.
[22] Long S, Ward IM. J Appl Polym Sci 1991;42:1921.
[23] Ryu DS, Osaki K. Polymer 1998;39:2515.
[24] Gordon DH, Duckett RA, Ward IM. Polymer 1994;35:2554.
[25] Buckley CP, Jones DC, Jones DP. Polymer 1996;37:2403.
[26] Sweeney J, Ward IM. Polymer 1995;36:299.
[27] Jabarin SA. Polym Engng Sci 1992;32:1341.
[28] Bassigny V, Seguela R, Rietsch F, Jasse B. Polymer 1993;34:4052.
[29] LeBourvellec G, Monnerie L, Jarry JP. Polymer 1986;27:856.
[30] Rao MVS, Kumar R, Dweltz NE. J Appl Polym Sci 1986;32:4439.